Environmental Research Letters

LETTER

Leading source and constraint on the systematic spread of the changes in East Asian and western North Pacific summer monsoon

Shijie Zhou[1,5], **Ping Huang**[1,2,4,6], **Gang Huang**[1,3,4,5,6] **and Kaiming Hu**[1,2,4]

[1] State key Laboratory of Numerical Modeling for Atmospheric Sciences and Geophysical Fluid Dynamics, Institute of Atmospheric Physics, Chinese Academy of Sciences, Beijing 100029, People's Republic of China
[2] Center for Monsoon System Research, Institute of Atmospheric Physics, Chinese Academy of Sciences, Beijing 100190, People's Republic of China
[3] Laboratory for Regional Oceanography and Numerical Modeling, Qingdao National Laboratory for Marine Science and Technology, Qingdao 266237, People's Republic of China
[4] Joint Center for Global Change Studies (JCGCS), Beijing 100875, People's Republic of China
[5] University of Chinese Academy of Sciences, Beijing 100049, People's Republic of China
[6] Author to whom any correspondence should be addressed.

E-mail: huangping@mail.iap.ac.cn **and** hg@mail.iap.ac.cn

Keywords: East Asian and western North Pacific summer monsoon, global warming, inter-model uncertainty, emergent constraint, CMIP5

Supplementary material for this article is available online

OPEN ACCESS

RECEIVED
11 August 2019

REVISED
1 November 2019

ACCEPTED FOR PUBLICATION
5 November 2019

PUBLISHED
11 December 2019

Abstract

With ongoing global warming, the changes in EA-WNPSM rainfall—feeding over two billion people in East Asia and the Indochina Peninsula—projected by the Coupled Model Intercomparison Project Phase 5 (CMIP5) models show remarkable and unidentified inter-model spread. Here, we reveal the leading inter-model spread of EA-WNPSM changes in 28 CMIP5 models is related to a 'dry north–wet south' dipole in East Asia and a wet Indochina and WNP. This spread pattern of EA-WNPSM changes is induced by the spread of sea surface temperature changes in the equatorial western Pacific, and can be further traced back to an apparent discrepancy among the state-of-the-art models in simulating the tropical Pacific rainfall. An air-sea coupling processes involved with summer background circulation contribute to this robust spread pattern of EA-WNPSM changes. We can constrain the EA-WNPSM rainfall changes based on the current-future relationship and observation that there should be more rainfall increase in North China and the Korean Peninsula and less increase in South China, the Indochina Peninsula and WNP, relative to previous multi-model ensemble projections.

1. Introduction

East Asian and western North Pacific summer monsoon (EA-WNPSM) is an essential part of the Asian-Australian monsoon system (Matsumoto 1997, Wang and Lin 2002, Ding and Chan 2005, Huang *et al* 2007, Wu *et al* 2012, Hsu *et al* 2014). Land–sea thermal contrast and Tibetan Plateau create the EA-WNPSM (Wu *et al* 2012), drawing abundant moisture from ocean to East Asia and Indochina Peninsula. Meanwhile, anomalous EA-WNPSM activities can induce droughts and floods, causing considerable economic losses and ecological damage (Huang *et al* 2007). Besides the natural fluctuations (Wang *et al* 2000), human influences such as the anthropogenic greenhouse-gas and aerosol emissions also play an important role in regulating the variation of EA-WNPSM from the recent decades (Menon *et al* 2002, Kitoh *et al* 2013).

Under global warming, the increase in atmospheric water vapor is believed to be responsible for an intensified global hydrological cycle (Held and Soden 2006, Durack *et al* 2012). Constrained by the radiative budget balance, weakened atmospheric circulation slows the increase in rainfall (Held and Soden 2006). For regional rainfall change, multiple controlling mechanisms that have not been fully understood hinder climate models to provide reliable projections (Xie *et al* 2015). Recent studies suggest an enhanced EA-WNPSM rainfall in climate model projections (Seo *et al* 2013, Lee and Wang 2014). However, the robust increase in EA-WNPSM rainfall (figure 1(a)) also shows remarkable inter-model spread on intensity and spatial pattern in state-of-the-art models

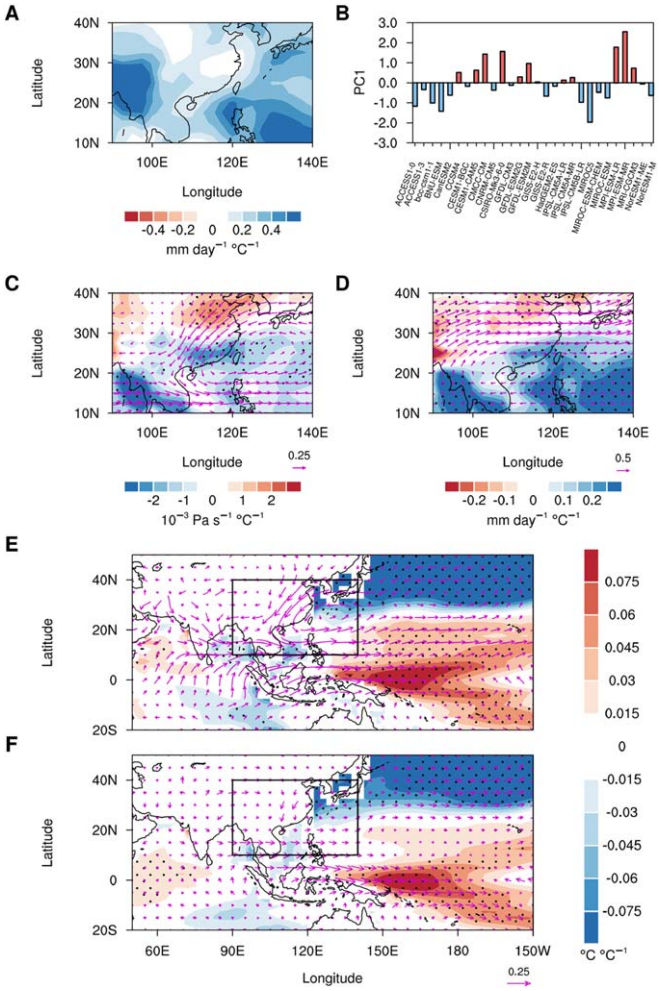

Figure 1. Inter-model regressions of future changes onto the normalized principal component (PC) of the first MV-EOF mode. (a) Multi-model ensemble (MME) of projection of rainfall change over the region of East Asia and western North Pacific summer monsoon in 28 CMIP5 models. (b) Normalized first PC of the MV-EOF analysis. (c) Changes in summer-mean (June–August) 500 hPa vertical pressure velocity (shaded) and 850 hPa winds (vectors; m s^{-1} $°C^{-1}$). (d) Changes in summer-mean rainfall (shaded) and 200 hPa winds (vectors; m s^{-1} $°C^{-1}$). (e) Changes in summer-mean SST (shaded) and 850 hPa winds (vectors). (f) Changes in annual-mean SST (shaded) and 850 hPa winds (vectors). The black rectangles in (e) and (f) denote the region (10°–40°N, 90°–140°E) where the MV-EOF analysis is performed. Stippling in (c)–(f) indicates the regressions are significant ($P < 0.05$) based on the Student's *t*-test.

(Christensen *et al* 2013, Kitoh *et al* 2013, Zhou *et al* 2018), mainly contributed by the large spread in projected circulation changes whose origins are as yet unidentified. The unclear formation of the EA-WNPSM change spread limits the development of climate models (Taylor *et al* 2012) and the application of emergent constraints (Boé *et al* 2009, Cox *et al* 2013, Huang and Ying 2015) to improve EA-WNPSM change projection. We reveal the leading mode of EA-WNPSM change spread is caused by a common bias in simulating the historical tropical rainfall. We also unravel the mechanism why their coupled relationship is only pronounced in boreal summer and prove it by numerical experiments.

2. Materials and methods

2.1. Models and data

We used the historical and Representative Concentration Pathway (RCP) 8.5 runs from 28 Coupled Model Intercomparison Project Phase 5 (CMIP5) models at http://pcmdi9.llnl.gov/ (Taylor *et al* 2012). They are ACCESS1.1, ACCESS1.3, BCC-CSM1.1, BNU-ESM, CanESM2, CCSM4, CESM1(BGC), CESM1(CAM5), CMCC-CM, CNRM-CM5, CSIRO-Mk3.6.0, GFDL-CM3, GFDL-ESM2G, GFDL-ESM2M, GISS-E2-H, GISS-E2-R, HadGEM2-ES, IPSL-CM5A-LR, IPSL-CM5A-MR, IPSL-CM5B-LR, MIROC5, MIROC-ESM, MIROC-ESM-CHEM, MPI-ESM-LR, MPI-ESM-MR, MRI-CGCM3, NorESM1-M and NorESM1-ME. See http://cmip-pcmdi.llnl.gov/cmip5/availability.html for details. In terms of observations, the rainfall data are from Global Precipitation Climatology Project (GPCP) version 2.3 dataset (Adler *et al* 2003) and the Climate Prediction Center (CPC) Merged Analysis of Precipitation (CMAP) dataset (Xie and Arkin 1997). The model outputs and observations were interpolated onto a 2.5° × 2.5° grid (from 90°S to 90°N, 0° to 357.5°E). ECHAM5, the fifth-generation atmospheric general

Table 1. Experiments using the ECHAM5 model.

Exp name	Description of the Exp design	Time
Exp_ctrl	The control run in a warming climate. It is forced by SST0 + SST1, in which SST0 is the observed monthly climatology of SST from the Taylor *et al* (2000) calculated as the long-term of the period from 1979 to 1996 and SST1 is a 2 °C uniform warming in the tropics (30°S–30°N)	31 years
Exp_annual	The first sensitivity run in a warming climate to illustrate the role of the regressed annual-mean tropical SST warming. It is forced by SST0 + SST1 + SST2, in which SST2 is an SST field with corresponding values to the regression pattern of annual-mean SST warming over the tropical Indo-Pacific region (20° S–25°N, 70°E–150°W) magnified ten times (figure S1 is available online at stacks.iop.org/ERL/14/124059/mmedia)	31 years
Exp_summer	The second sensitivity run in a warming climate to illustrate the role of the regressed monthly tropical SST warming. It is forced by SST0 + SST1 + SST3, in which SST3 is the same as SST2 but for the monthly SST warming with seasonal cycle (figure S2)	31 years
Exp_annual_60N	The third sensitivity run in a warming climate to illustrate the role of the regressed annual-mean SST warming extending to high latitudes. It is forced by SST0 + SST1 + SST4, in which SST4 (figure S3) is similar to SST2 but extending north to 60°N (20°S–60°N, 70°E–150°W)	31 years

circulation model developed at the Max Planck Institute for Meteorology (Roeckner *et al* 2003), was chosen in this study for the atmospheric experiments because of its high skill in simulating the East Asian summer monsoon (EASM; Zhou *et al* 2009b).

2.2. Climatology and change

The 1981–2000 mean in historical runs defined the present-day climatology, the 2079–2098 mean in the RCP 8.5 runs defined the future climatology, and their difference represented the change under global warming. The multi-model ensemble (MME) was defined as the simple average of the 28 models. The summer mean was defined as the average of June–August. The variables used included the sea surface temperature (SST), precipitation, net surface short-wave radiation flux, net surface long-wave radiation flux, surface latent heat flux, surface sensible heat flux, zonal and meridional winds at 1000, 850 and 200 hPa, surface scalar wind speed and vertical pressure velocity at 500 hPa. Analyses related to surface scalar wind speed were based on 24 of the 28 models, excluding CCSM4, CESM1(BGC), NorESM1-M and NorESM1-ME, as this variable is unavailable in these four models. To remove the effect of inter-model uncertainty from the global mean temperature change, all the future changes in this study were normalized by the global mean temperature increase in respective models.

2.3. Multivariate empirical orthogonal function

Multivariate empirical orthogonal function (MV-EOF) is an extended method based on the conventional EOF (Wang 1992), which builds a combined data matrix for the selected variables before conventional EOF analysis and thus can capture the dominant spatial relationship among various variable fields. In this study, the MME value of each variable among the 28 models is first removed from each model before the inter-model MV-EOF, and then each variable is divided by the standard deviation of that variable field to analyze coherent variations of all variables.

2.4. Numerical experiments using the ECHAM5 model

To verify the formation of the EA-WNPSM circulation response and to clarify the relative contributions of seasonal background circulation and the air–sea positive feedback in section 3.2, we performed four sets of numerical experiments using the ECHAM5 model (Roeckner *et al* 2003), one control run (Exp_ctrl) and three sensitivity runs (Exp_annual, Exp_summer and Exp_annual_60N). The details of experiment design were listed in table 1. We ran each experiment for 31 years and extracted the mean of the last 30 years for analysis.

2.5. Historical tropical Pacific rainfall index

To quantify the extent of model simulation and observation associated with regression pattern of tropical Pacific rainfall, we defined a historical tropical Pacific rainfall index. It was calculated by projecting the deviation of historical rainfall in a model or observation from the MME simulated historical rainfall onto the regression pattern of tropical Pacific rainfall over the tropical Pacific region (20°S–20°N, 120°E–70°W), which is shown in section 3.4. The deviations of observed rainfall (GPCP and CMAP) from MME simulated rainfall were also projected onto the regressed rainfall pattern to represent the observation, as shown by the vertical red and blue solid lines.

2.6. Local kinetic energetics analyses

The development of the perturbed kinetic energy (KE) response to external forcing is dependent on the background dynamics. The KE $[(u'^2 + v'^2)/2]$ converted from the background circulation is based on the following formulas (Kosaka and Nakamura 2006, Hu *et al* 2019):

$$\frac{\partial\left[\frac{u'^2+v'^2}{2}\right]}{\partial t} \approx \underbrace{\frac{(v'^2-u'^2)}{2}\left(\frac{\partial u_b}{\partial x}-\frac{\partial v_b}{\partial y}\right)}_{CKx} - \underbrace{u'v'\left(\frac{\partial u_b}{\partial y}+\frac{\partial v_b}{\partial x}\right)}_{CKy}, \quad (1)$$

where u' and v' are the anomalous 850 hPa zonal and meridional winds, u_b and v_b are the present-day climatological summer-mean winds at 850 hPa, CKx represents the conversion of KE from a mean confluent flow to perturbations and CKy represents the conversion from a mean horizontal shear to perturbations.

2.7. Surface energy budget decompositions

The ocean surface energy budget balance is an efficient method to investigate the formation mechanism of SST patterns (Xie *et al* 2010). The energy budget balance in the mixed layer ocean can be expressed as:

$$\rho_0 C_P h\frac{\partial \Delta T}{\partial t} = \Delta Q_L + \Delta Q_S + \Delta Q_E + \Delta Q_H + \Delta D_o, \quad (2)$$

where Δ denotes the future change, ρ_0 and C_P are the density and specific heat of seawater, h is the depth of the mixed layer, T is the SST, $\rho_0 C_P h\frac{\partial \Delta T}{\partial t}$ is the tendency of heat content in the mixed layer hereafter referred as to ΔQ_t, Q_L is the net surface long-wave radiation flux, Q_S is the net surface short-wave radiation flux, Q_E is the surface latent heat flux, Q_H is the surface sensible heat flux and D_o is the ocean heat transport convergence. Positive heat fluxes (Q_L, Q_S, Q_E, Q_H, D_O) are defined as warming the ocean. We used a constant mixed layer (h) of 50 m in this study to make sure that the results were not sensitive to the seasonal variation of the mixed-layer depth (Dwyer *et al* 2012). In this study, we focused on the summer mean of $\Delta Q_t = \rho_0 C_P h\frac{\partial \Delta T}{\partial t}$ and used the difference between the ΔT in May and August in the calculation of $\frac{\partial \Delta T}{\partial t}$.

Following previous studies (Du and Xie 2008, Xie *et al* 2010), the latent heat flux change ΔQ_E in equation (2) can be decomposed into three components:

$$\Delta Q_E = \Delta Q_{EO} + \Delta Q_{EW} + \Delta Q_{E-others}, \quad (3)$$

where ΔQ_{EO} denotes the effect of SST change, ΔQ_{EW} denotes the effect of surface wind speed (W) change, calculated as $\Delta Q_{EW} = Q_E\frac{\Delta W}{W}$, and $\Delta Q_{E-others}$ is a residual that represents the effect of relative humidity and stability change.

3. Results

3.1. The leading systematic spread of EA-WNPSM change

The leading mode of the inter-model spread in EA-WNPSM circulation changes was extracted by a MV-EOF analysis performed on a set of five circulation variables, including the changes in zonal and meridional winds at 850 hPa and 200 hPa and the vertical pressure velocity at 500 hPa, in boreal summer mean (June–August) in the EA-WNPSM region (10°–40°N, 90°–140°E) similar to (Wang *et al* 2008). The first mode of the inter-model MV-EOF accounts for 30.3% of the total variance of EA-WNPSM. The regression patterns of EA-WNPSM changes onto the normalized first principal component (PC1; figure 1(b)) show a conspicuous meridional dipole pattern of changes in 500 hPa vertical pressure velocity (figure 1(c)) associated with 'dry north–wet south' rainfall (figure 1(d)), a cyclonic pattern of lower-level circulation changes (figure 1(c)), and a southward shift in the upper-level jet stream (figure 1(d)) for EASM, and a pattern of lower-level westerly changes with enhanced rainfall for WNPSM. The meridional dipole pattern of EASM is similar to the well-known pattern of the interdecadal variation of EASM rainfall (Gong and Ho 2002, Ding *et al* 2008, Zhou *et al* 2009a, Wu *et al* 2019). (For EOF analysis, the patterns of EOF1 in figures 1(c) and (d) with the normalized PC in figure 1(b) are equivalent to a pattern with a PC of opposite sign. To simplify the presentation, we describe EOF1 as in figures 1(c) and (d) and all patterns in the following analyses are regressed onto the associated PC1 in figure 1(b).)

Previous studies have suggested that the inter-model spread of some major components of Asian monsoon change can be attributed to the uncertainty in tropical SST warming (Yang and Lau 1998, Yun *et al* 2010, Chen and Zhou 2015, Li *et al* 2017). The regressed summer-mean tropical SST changes onto PC1 appear to be significant and positive—indicating more SST warming—in the equatorial western Pacific, but negative in the eastern Indian Ocean, Maritime Continent region and South China Sea (figure 1(e)). A broader view (only for regression pattern, not for the region of MV-EOF analysis) of the regressed 850 hPa winds (figure 1(e)) shows that the lower-level cyclonic pattern of EASM and the westerlies of WNPSM in figure 1(c) seem to be part of a Gill-type circulation response to warming SST in the equatorial western Pacific (Gill 1980).

On close inspection, the Gill-type circulation response is asymmetric, being stronger north than south of the equator. Moreover, the regressed summer-mean SST changes (figure 1(e)) are almost equal to the annual mean in the equatorial western Pacific, but stronger than the annual mean in the Asian-Pacific summer monsoon region (figures 1(f) and S4).

Meanwhile, the summer circulation (EA-WNPSM) response is much stronger than the annual mean (figure S4). But why is the spread of EA-WNPSM and monsoon-region SST changes more pronounced in summer, and where does the annually consistent spread of equatorial western Pacific SST changes originate from?

3.2. Mechanisms of stronger circulation response in boreal summer

A local kinetic energetics analysis was performed to understand the enlarged spread of EA-WNP circulation in summer, which is an efficient method to reveal the conversion of local KE from background circulation (Kosaka and Nakamura 2006, Hu *et al* 2019). In summer, the lower-level monsoon westerlies from the North Indian Ocean and the prevailing easterly trades over the Northwest Pacific form a confluent zone over the Indo-Northwest Pacific region (figure S5). Such a confluent zone favors zonally elongated perturbations to gain KE from the mean flow (Kosaka and Nakamura 2006), equaling a positive conversion of local KE from the mean flow. As theoretically expected, positive conversion is distributed from the Bay of Bengal to the Luzon Islands in the Philippines (figures 2(a) and (b)) when the westerlies of the EA-WNP response appear in the confluent zone. The Indo-western Pacific westerlies (u') of the regressed EA-WNPSM circulation change weakens the zonal gradient of zonal mean state momentum $\left(\frac{\partial u_b}{\partial x}\right)$ in the confluent zone (figure S5), and gains KE from the mean flow, which contributes most to the positive conversion. The similar magnitudes of KE induced by westerlies (u') in figure 2(b) and total conversion of KE in figure 2(a) verify this assumption. The positive KE conversion in turn strengthens westerly anomalies and makes them peak around 10°–15°N at 850 hPa. The enhanced westerly anomalies could lead to surface convergence in the southern EASM region (figure 2(c)) via the effect of Ekman friction (Xie *et al* 2009). The convergence induced by westerly anomalies facilitates convection and the resultant diabatic heating can in turn promote the development of EA-WNP circulation (Xie *et al* 2009). In short, the summer background circulation creates a more pronounced EA-WNP circulation response to equatorial western Pacific SST warming in summer.

The apparent EA-WNP circulation response to SST warming in summer can feed back to SST in the monsoon regions, which could lead to a larger zonal SST gradient in the tropical Indo-western Pacific in summer (figures 1(e) and (f)) and enlarge the EA-WNPSM response. In the sea surface energy budget analysis, the regressed tendency of summer-mean changes in mixed layer heat storage (ΔQ_t; figure 3(a)) are positive over the WNP and negative from the tropical eastern Indian Ocean to the South China Sea, which indicates an increased zonal SST gradient in summer relative to the annual mean. This pattern is very similar to the regressed summer variation (the departure of the summer mean from annual mean) of changes in latent heat flux induced by the surface wind speed (ΔQ_{EW}; figure 3(b)), whereas the other surface energy budgets terms contribute little (figure S6). Clearly, the ΔQ_{EW} in figure 3(b) is the result of low-level wind spread changes lead by the EA-WNPSM wind changes (figure 1(e)) on the background EA-WNPSM circulation (figure S5). The Indo-western Pacific westerlies of the regressed EA-WNPSM circulation change (contours in figure 3(c)) strengthen the monsoonal westerlies over the Northeast Indian Ocean and the South China Sea and weaken the prevailing easterlies over the WNP (shaded in figure 3(c)). In summary, the original SST warming in the equatorial western Pacific with the summer background circulation can arouse a remarkable air–sea positive feedback to strengthen the zonal gradient of SST warming in the EA-WNPSM region and the EA-WNPSM circulation response.

3.3. Numerical experiments

As summarized in table 1, four sets of numerical experiments using the atmospheric general circulation model ECHAM5 were performed to verify the formation of the EA-WNPSM circulation response and to clarify the relative contributions of seasonal background circulation and the air–sea positive feedback. As shown in figure 4, the experiments reproduce the Gill-type response to the equatorial western Pacific SST warming well, albeit with a somewhat southward shift of the cyclonic circulation response in the EASM region compared to that in figure 1(e), probably due to the lack of air-sea interaction in the atmospheric model (Song and Zhou 2014). In both Exp_annual and Exp_summer, the circulation response over the EA-WNPSM region is obviously stronger in summer than other seasons (figures 4(a)–(d)), and a relatively large zonal SST warming gradient in summer in Exp_summer can indeed intensify the EA-WNPSM circulation response (figure 4(c)) relative to that in Exp_annual (figure 4(a)). The role of the background EA-WNPSM circulation can be measured by the difference between the summer-mean and annual-mean response in Exp_annual (figure 4(a) minus figure 4(b)), shown in figure 4(e), and the role of the enlarged zonal SST gradient in summer can be measured by the difference between the summer response in Exp_summer and Exp_annual (figure 4(c) minus figure 4(a)), shown in figure 4(f). It can be concluded that the two mechanisms are approximately equal for the EASM response, but the role of background circulation is dominant for the WNPSM response. Although there are significant SST signals in the North Pacific (figures 1(e) and (f)), the EA-WNPSM response in the sensitivity experiment Exp_annual_60N (table 1) is very close to that in Exp_annual (figure S7), indicating the role of the

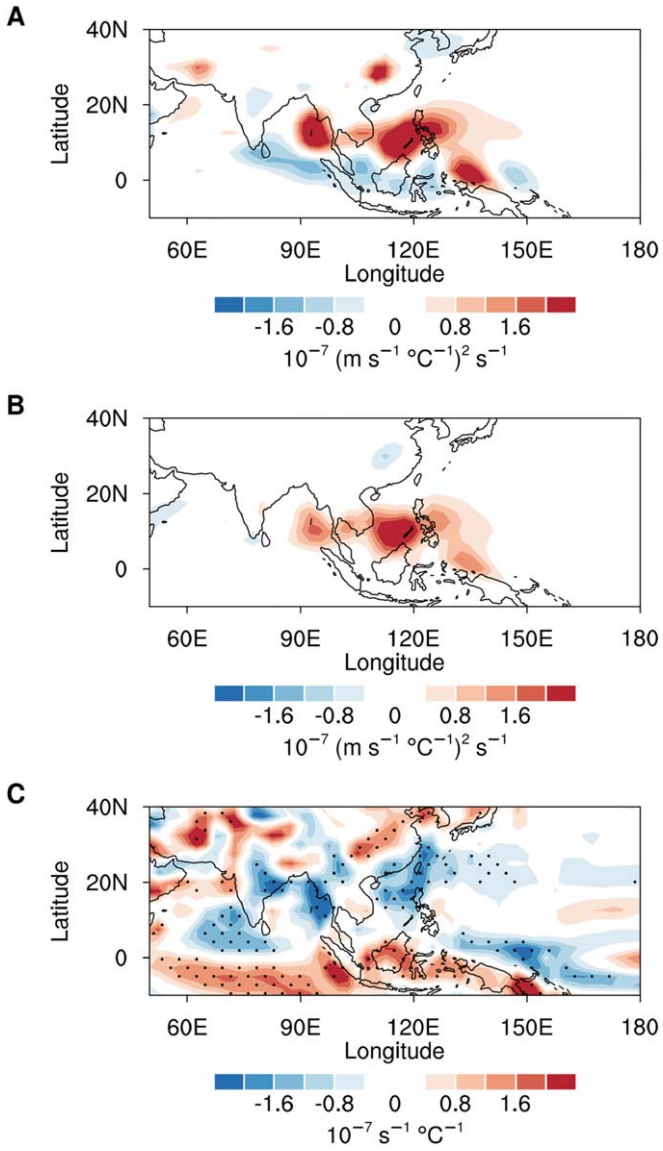

Figure 2. Local atmospheric kinetic energy conversion. (a) Conversion of KE ($(m\,s^{-1}\,°C^{-1})^2\,s^{-1}$) from the basic flow to wind anomalies at 850 hPa in summer. (b) Conversion of KE ($(m\,s^{-1}\,°C^{-1})^2\,s^{-1}$) from the zonal basic flow to zonal wind anomalies. (c) Inter-model regression pattern of changes in summer-mean 1000 hPa divergence onto the normalized PC1. Stippling in (c) indicates that the regressions are significant ($P < 0.05$) based on the Student's *t*-test.

North Pacific SST (regions (30°N–60°N, 150°E–150° W) in figures 1(e) and (f)) in the EA-WNPSM response is negligible.

3.4. Original bias in historical simulation of tropical rainfall

To further trace the source of the annually persistent western Pacific SST change spread, we analyzed the regressed annual-mean changes in the sea surface energy budget. The only term with a positive contribution to the annually persistent western Pacific SST changes is the surface net shortwave flux change (figure 5(a); and other terms shown in figure S8). Although the location of the surface net shortwave flux change is not well consistent with that of the SST changes, it can be well explained by a mechanism proposed in Ying and Huang (2016). The relatively strong surface net shortwave flux over the central Pacific can directly lead to a warm SST deviation over the central Pacific; then this warm SST deviation can induce a low-level convergence that suppresses (enhances) the evaporative cooling and zonal cold advection in the western (eastern) Pacific because of the prevailing easterly trades over the tropical Pacific; and finally the original warm SST deviation directly induced by the shortwave flux change in the central Pacific will move westward to the western Pacific (Ying and Huang 2016). Previous studies have suggested that the sensitive convection response to surface warming in the convective region can suppress local surface warming by modulating the surface net shortwave flux (Ramanathan and Collins 1991), which is one of the most remarkable mechanisms forming the spatial pattern of global SST warming. This mechanism implies that the spread of the equatorial western Pacific SST change and the associated net shortwave

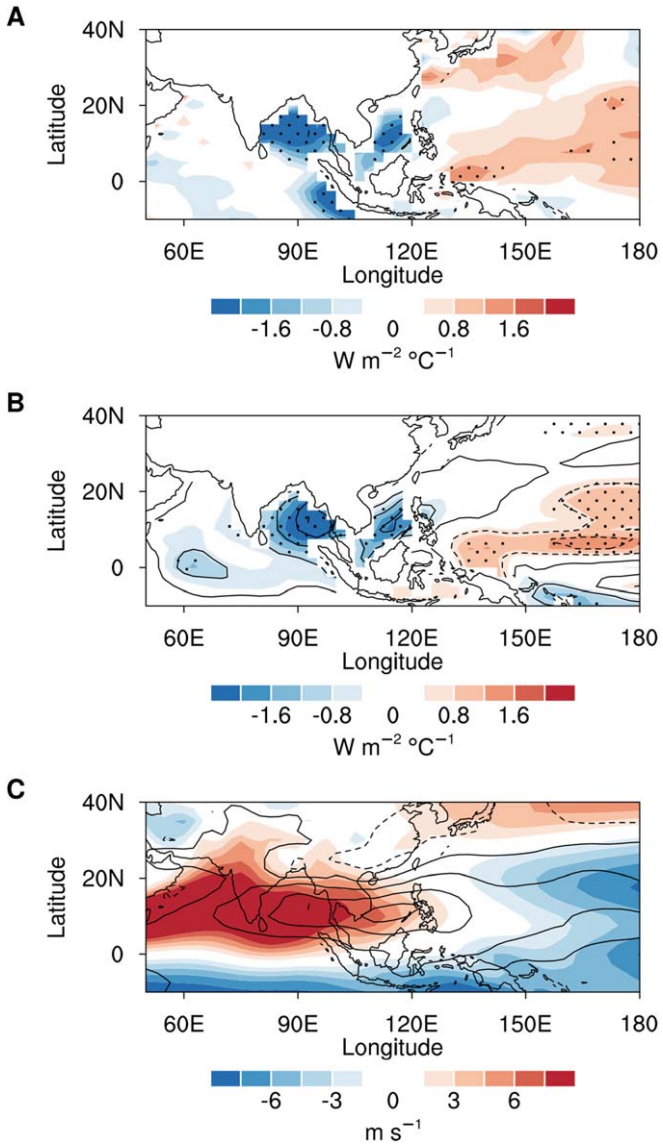

Figure 3. Sea surface energy budget analyses. (a) Regression of the tendency of summer-mean changes in mixed layer heat storage (shaded) onto PC1. (b) Regression of summer variation of changes in the latent heat flux induced by the surface wind speed changes (shaded), and the percentage changes of surface wind speed relative to the climatological surface wind speed (contours; intervals of 0.5%; negative values dashed) onto PC1. (c) Present-day summer zonal wind climatology (m s^{-1}) at 850 hPa in multi-model mean (shaded) and inter-model regression pattern of changes in summer-mean zonal wind at 850 hPa onto the normalized PC1 (contours; intervals of 0.1 m s^{-1} $°C^{-1}$; negative values dashed). Stippling in (a) and (b) indicates that the regressions are significant ($P < 0.05$) based on the Student's *t*-test.

flux change could originate from the spread of convective activity in the tropical Pacific among the models. This hypothesis is confirmed by the significant regressed historical rainfall representing convective activity (figure 5(b)). In the models with less historical rainfall (around 5°S–5°N; figure 5(b)), the western Pacific convection cannot suppress surface greenhouse warming as much as the MME, and thus these models project larger surface warming in the equatorial western Pacific (figure 1(f)).

Based on the historical rainfall in the tropical Pacific as the source of the leading inter-model spread of EA-WNPSM changes, we can narrow the uncertainty of EA-WNPSM changes in MME projection by emergent constraints (Boé *et al* 2009, Cox *et al* 2013, Huang and Ying 2015, Hall *et al* 2019). Emergent constraint is based on an implicit relationship (f) between elements of current (X) and future (Y) climate among 28 CMIP5 models, that is $Y = f(X) + \varepsilon$, in which ε is a small departure from f. In this study, X is the regression pattern of annual-mean rainfall on PC1, Y is the PC1 of inter-model MV-EOF. Their relationship (f) was proved in figure 5(c). We define the historical tropical Pacific rainfall index to quantify X and applied it on the bias of X so that we can place this constraint on Y, the PC1 of inter-model MV-EOF (Hall *et al* 2019). This index is significantly correlated with PC1 (figure 5(c); inter-model correlation 0.77), consistent with the widely significant regression in figure 5(b). Relative to the MME simulation in the CMIP5 models,

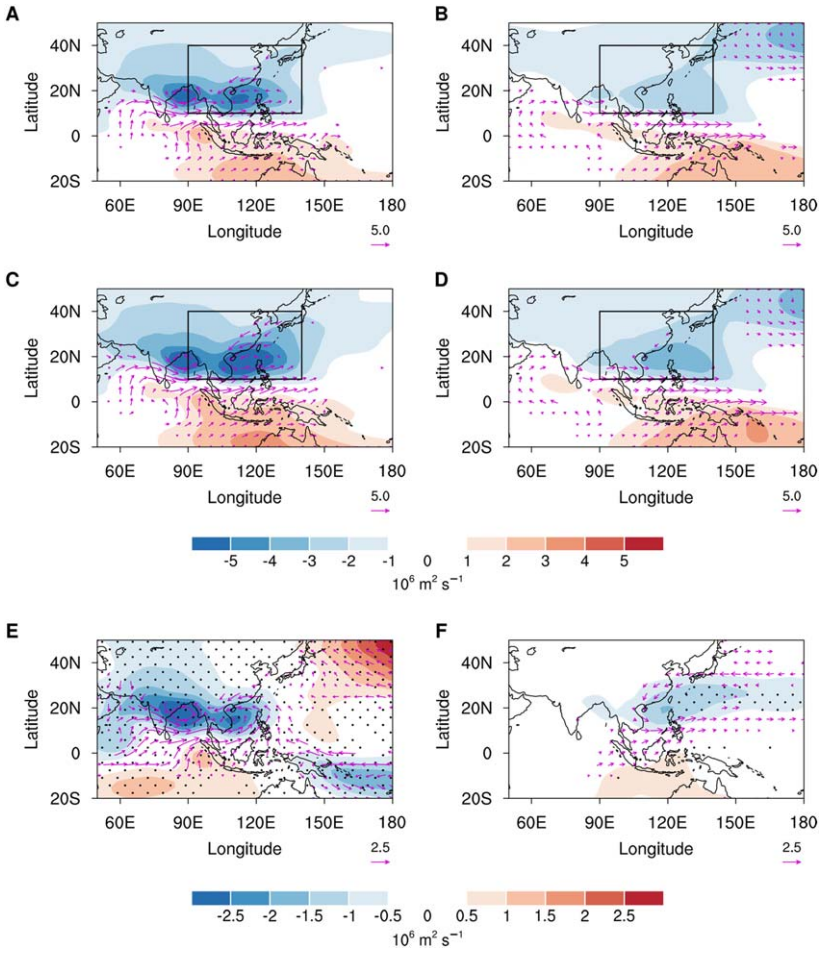

Figure 4. Atmospheric response to Indo-western Pacific SST warming in the ECHAM5 sensitivity experiments. The (a) summer-mean and (b) annual-mean 850 hPa winds (vectors) and streamfunction (shaded) in the difference of the atmospheric response between Exp_annual and the control run Exp_ctrl. (c) and (d) as in (a) and (b), but for the difference between Exp_summer and Exp_ctrl. (e) Differences between (a) and (b), and (f) the differences between (a) and (c). The black rectangles in (a) and (d) denote the EA-WNPSM region as in figure 1(e). Stippling in (e) and (f) indicates that the differences are significant ($P < 0.05$) based on the Student's *t*-test.

the rainfall should realistically be stronger in the equatorial central Pacific but weaker in the flanks (figure S9) (Mechoso *et al* 1995, Dai 2006, Lin 2007), which are well-known tropical Pacific rainfall biases in these state-of-the-art models. Thus, the rainfall indexes for the observations (red and blue solid lines shown figure 5(c)) are negative when the MME simulated rainfall is zero in the index definition. Their corresponding values of PC1 predicting from the relationship between PC1 and rainfall coefficients are shown as dash lines in figure 5(c). Relatively low PC1 values predicting from observed rainfall indexes suggest that the pattern of EA-WNPSM rainfall changes as in figure 1(d), 'dry north–wet south', is overestimated in the MME projection (figure 1(a)). Thus, we can constrain the EA-WNPSM rainfall change that the rainfall increase should be raised in North China and the Korean Peninsula but lowered in South China, the Indochina Peninsula and the WNP, relative to the MME projection. However, we should also notice that the so-called observations from different sources (GPCP and CMAP) show apparent discrepancies in the tropical Pacific (figures 5(c) and S9), implying it is still crucial in the future to improve observations and understanding with respect to present-day tropical Pacific rainfall.

4. Conclusions

In this study, we found a systematic spread of EA-WNPSM changes under global warming projected by the CMIP5 models, and traced the systematic mode back to the inter-model discrepancy in simulating the present-day rainfall in the equatorial western Pacific. Under global warming, one model with less historical rainfall (implying weaker convection activity) in the equatorial Pacific cannot suppress the local surface warming by the cloud-shortwave negative feedback as much as the MME, leading to a greater surface warming in the equatorial western Pacific. We found that this surface warming is annually persistent, however, it can couple with summer background circulation to induce a systematic spread of EA-WNPSM changes. In boreal summer, this SST

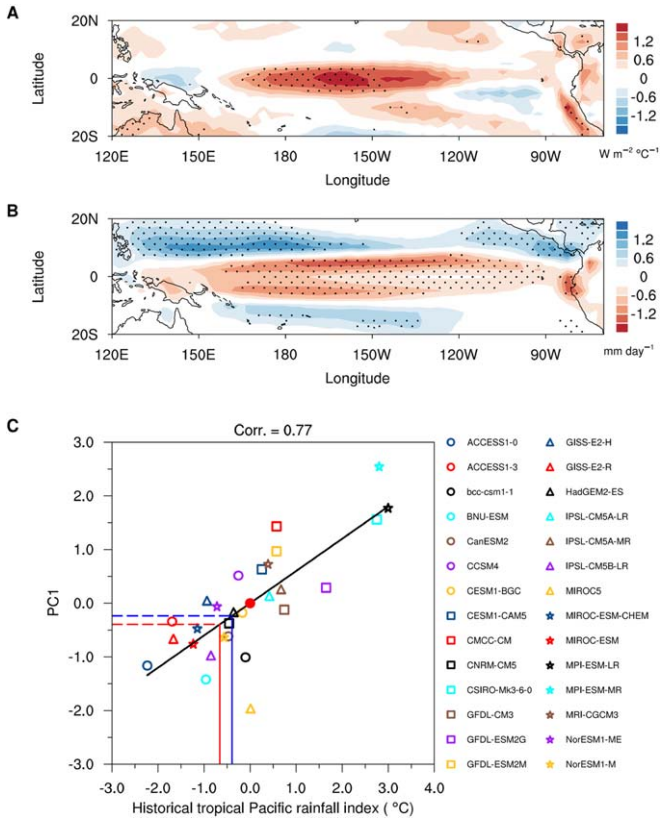

Figure 5. Tropical Pacific short-wave flux change, historical rainfall and constraints for EA-WNPSM changes. (a) Inter-model regression of annual-mean changes in surface net short-wave flux onto PC1. (b) Regression of the annual-mean rainfall in historical runs onto PC1. (c) Relationship between PC1 and historical tropical Pacific rainfall index in the 28 models. The inter-model correlation coefficient is shown at the top of the panel and is significant ($P < 0.01$) based on the Student's t-test. Stippling in (a) and (b) indicates the regressions are significant ($P < 0.05$) based on the Student's t-test. The red and blue solid lines in (c) denote the historical tropical Pacific rainfall indexes of the observed rainfall (red for GPCP and blue for CMAP) with dash lines for corresponding values of PC1 based on the relationship shown in (c).

warming can force a more apparent Gill-type atmospheric response in the Indo-western Pacific than in other seasons, appearing as a 'dry north–wet south' dipole in East Asia and wet in Indochina and WNP, in which the *KE* converted from the summer background circulation and the enlargement of the consequent air–sea interaction are the two key processes. Considering the common double-ITCZ bias of tropical Pacific rainfall in state-of-the-art models (Mechoso *et al* 1995, Dai 2006, Lin 2007), we can constrain the EA-WNPSM rainfall changes that there should be more rainfall increase in North China and the Korean Peninsula and less increase in South China, the Indochina Peninsula and WNP compared to previous MME projections. This result suggests an effective way for a more reliable EA-WNPSM projection by improving our understanding and simulation of the tropical Pacific convection and rainfall.

Acknowledgments

We acknowledge the World Climate Research Programme's Working Group on Coupled Modeling, which is responsible for CMIP5, and the climate modeling groups for producing and making available their model output. We also thank two anonymous reviewers for their constructive suggestions.

Funding

This work was supported by the National Key R&D Program of China (Grant 2019YFA0606703), the National Natural Science Foundation of China (Grants 41975116, 41722504 and 41831175), the Youth Innovation Promotion Association CAS (2016074), and the Fundamental Research Funds for the Central Universities.

Data availability

The data that support the finding of this study are openly available at CMIP5 http://pcmdi9.llnl.gov/ (Taylor *et al* 2012), GPCP precipitation (Adler *et al* 2003), and CMAP precipitation (Xie and Arkin 1997).

ORCID iDs

Kaiming Hu https://orcid.org/0000-0002-9988-5747

References

Adler R F *et al* 2003 The version-2 global precipitation climatology project (GPCP) monthly precipitation analysis (1979–present) *J Hydrometeorol.* **4** 1147–67

Boé J, Hall A and Qu X 2009 September sea-ice cover in the Arctic ocean projected to vanish by 2100 *Nat. Geosci.* **2** 341–3

Chen X and Zhou T 2015 Distinct effects of global mean warming and regional sea surface warming pattern on projected uncertainty in the South Asian summer monsoon *Geophys. Res. Lett.* **42** 9433–9

Christensen J H *et al* 2013 Climate phenomena and their relevance for future regional climate change *Climate Change 2013: The Physical Science Basis* ed T F Stocker *et al* (Cambridge: Cambridge University Press) IPCC 1217–308

Cox P M, Pearson D, Booth B B, Friedlingstein P, Huntingford C, Jones C D and Luke C M 2013 Sensitivity of tropical carbon to climate change constrained by carbon dioxide variability *Nature* **494** 341

Dai A 2006 Precipitation characteristics in eighteen coupled climate models *J. Clim.* **19** 4605–30

Ding Y and Chan J C L 2005 The East Asian summer monsoon: an overview *Meteorol. Atmos. Phys.* **89** 117–42

Ding Y, Wang Z and Sun Y 2008 Inter-decadal variation of the summer precipitation in east China and its association with decreasing Asian summer monsoon: I. Observed evidences *Int. J. Climatol.* **28** 1139–61

Du Y and Xie S-P 2008 Role of atmospheric adjustments in the tropical Indian Ocean warming during the 20th century in climate models *Geophys. Res. Lett.* **35** L08712

Durack P J, Wijffels S E and Matear R J 2012 Ocean salinities reveal strong global water cycle intensification during 1950 to 2000 *Science* **336** 455–8

Dwyer J G, Biasutti M and Sobel A H 2012 Projected changes in the seasonal cycle of surface temperature *J. Clim.* **25** 6359–74

Gill A E 1980 Some simple solutions for heat-induced tropical circulation *Q. J. R. Meteorol. Soc.* **106** 447–62

Gong D-Y and Ho C-H 2002 Shift in the summer rainfall over the yangtze river valley in the late 1970s *Geophys. Res. Lett.* **29** 78-1–4

Hall A, Cox P, Huntingford C and Klein S 2019 Progressing emergent constraints on future climate change *Nat. Clim. Change* **9** 269–78

Held I M and Soden B J 2006 Robust responses of the hydrological cycle to global warming *J. Clim.* **19** 5686–99

Hsu H-H, Zhou T and Matsumoto J 2014 East Asian, indochina and western North Pacific summer monsoon—an update *Asia-Pac. J. Atmos. Sci.* **50** 45–68

Hu K, Huang G, Xie S-P and Long S-M 2019 Effect of the mean flow on the anomalous anticyclone over the Indo-northwest Pacific in post-El Niño summers *Clim. Dyn.* **53** 5725–41

Huang P and Ying J 2015 A multimodel ensemble pattern regression method to correct the tropical Pacific SST change patterns under global warming *J. Clim.* **28** 4706–23

Huang R, Chen J and Huang G 2007 Characteristics and variations of the East Asian monsoon system and its impacts on climate disasters in China *Adv. Atmos. Sci.* **24** 993–1023

Kitoh A, Endo H, Krishna Kumar K, Cavalcanti I F A, Goswami P and Zhou T 2013 Monsoons in a changing world: a regional perspective in a global context *J. Geophys. Res. Atmos.* **118** 3053–65

Kosaka Y and Nakamura H 2006 Structure and dynamics of the summertime Pacific–Japan teleconnection pattern *Q. J. R. Meteorol. Soc.* **132** 2009–30

Lee J-Y and Wang B 2014 Future change of global monsoon in the CMIP5 *Clim. Dyn.* **42** 101–19

Li G, Xie S-P, He C and Chen Z 2017 Western Pacific emergent constraint lowers projected increase in Indian summer monsoon rainfall *Nat. Clim. Change* **7** 708–12

Lin J-L 2007 The double-ITCZ problem in IPCC AR4 coupled GCMs: Ocean–atmosphere feedback analysis *J. Clim.* **20** 4497–525

Matsumoto J 1997 Seasonal transition of summer rainy season over indochina and adjacent monsoon region *Adv. Atmos. Sci.* **14** 231–45

Mechoso C R *et al* 1995 The seasonal cycle over the tropical Pacific in coupled ocean–atmosphere general circulation models *Mon. Weather Rev.* **123** 2825–38

Menon S, Hansen J, Nazarenko L and Luo Y 2002 Climate effects of black carbon aerosols in China and India *Science* **297** 2250–3

Ramanathan V and Collins W 1991 Thermodynamic regulation of ocean warming by cirrus clouds deduced from observations of the 1987 El Niño *Nature* **351** 27–32

Roeckner E *et al* 2003 The atmospheric general circulation model ECHAM 5: I. Model description *Report* 349 Max Planck Institute for Meteorology

Seo K H, Ok J, Son J H and Cha D H 2013 Assessing future changes in the East Asian summer monsoon using CMIP5 coupled models *J. Clim.* **26** 7662–75

Song F and Zhou T 2014 Interannual variability of East Asian summer monsoon simulated by CMIP3 and CMIP5 AGCMs: Skill dependence on Indian Ocean–western Pacific anticyclone teleconnection *J. Clim.* **27** 1679–97

Taylor K E, Stouffer R J and Meehl G A 2012 An overview of CMIP5 and the experiment design *Bull. Am. Meteor. Soc.* **93** 485–98

Taylor K E, Williamson D and Zwiers F 2000 The sea surface temperature and sea-ice concentration boundary conditions for amip II simulations *PCMDI Report No.* 60 program for climate model diagnosis and intercomparison, Lawrence Livermore National Laboratory

Wang B 1992 The vertical structure and development of the ENSO anomaly mode during 1979–1989 *J. Atmos. Sci.* **49** 698–712

Wang B and Lin H 2002 Rainy season of the Asian–Pacific summer monsoon *J. Clim.* **15** 386–98

Wang B, Wu R and Fu X 2000 Pacific–East Asian teleconnection: How does ENSO affect East Asian climate? *J. Clim.* **13** 1517–36

Wang B, Wu Z, Li J, Liu J, Chang C-P, Ding Y and Wu G 2008 How to measure the strength of the East Asian summer monsoon *J. Clim.* **21** 4449–63

Wu G, Liu Y, He B, Bao Q, Duan A and Jin F F 2012 Thermal controls on the Asian summer monsoon *Sci. Rep.* **2** 404

Wu R, You T and Hu K 2019 What formed the North–South contrasting pattern of summer rainfall changes over eastern China? *Curr. Clim. Change Rep.* **5** 47–62

Xie P and Arkin P A 1997 Global precipitation: a 17-year monthly analysis based on gauge observations, satellite estimates, and numerical model outputs *Bull. Am. Meteor. Soc.* **78** 2539–58

Xie S-P, Deser C, Vecchi G A, Ma J, Teng H and Wittenberg A T 2010 Global warming pattern formation: sea surface temperature and rainfall *J. Clim.* **23** 966–86

Xie S-P, Hu K, Hafner J, Tokinaga H, Du Y, Huang G and Sampe T 2009 Indian Ocean capacitor effect on Indo–western Pacific climate during the summer following El Niño *J. Clim.* **22** 730–47

Xie S-P *et al* 2015 Towards predictive understanding of regional climate change *Nat. Clim. Change* **5** 921–30

Yang S and Lau K M 1998 Influences of sea surface temperature and ground wetness on Asian summer monsoon *J. Clim.* **11** 3230–46

Ying J and Huang P 2016 Cloud–radiation feedback as a leading source of uncertainty in the tropical Pacific SST warming pattern in CMIP5 models *J. Clim.* **29** 3867–81

Yun K-S, Ha K-J and Wang B 2010 Impacts of tropical ocean warming on East Asian summer climate *Geophys. Res. Lett.* **37** L20809

Zhou S, Huang G and Huang P 2018 Changes in the East Asian summer monsoon rainfall under global warming: moisture budget decompositions and the sources of uncertainty *Clim. Dyn.* **51** 1363–73

Zhou T, Gong D, Li J and Li B 2009a Detecting and understanding the multi-decadal variability of the East Asian summer monsoon recent progress and state of affairs *Meteorol. Z.* **18** 455–67

Zhou T, Wu B and Wang B 2009b How well do atmospheric general circulation models capture the leading modes of the interannual variability of the Asian–Australian monsoon? *J. Clim.* **22** 1159–73